

X-RAY AND RAMAN STUDIES OF MeV ION-BOMBARDED GaInAs/GaAs

Chu R. WIE

State University of New York at Buffalo, Department of Electrical and Computer Engineering, 201 Bonner Hall, Amherst, New York 14260, USA

G. BURNS, F.H. DACOL, G.D. PETTIT and J.M. WOODALL

IBM T.J. Watson Research Center, Yorktown Heights, New York 10598, USA

Received 27 February 1989 and in revised form 22 May 1989

We have measured elastic strains and longitudinal optical (LO) phonon shifts in MeV ion-bombarded single layers of (GaIn)As on GaAs(001). We have used He, P, and Cl ions, all in the MeV range, to bombard the samples. Unexpectedly, it is found that the elastic strains initially decrease and the LO phonon frequency initially increases with dose. At higher doses, the strain increases and phonon frequency decreases, as expected for damaged GaAs crystals. For layers with negligible lattice relaxation (i.e., with an in-plane mismatch less than 0.01%), a precipitous perpendicular strain release occurs at a high damage-energy deposition level. The in-plane mismatch for these samples, however, did not change over the same dose range. For 1 μm thick, well-relaxed layers, the ion-beam-induced strain and phonon shift behave similarly to those in ion-damaged bulk GaAs crystals.

1. Introduction

Lattice mismatched strained heterojunction (GaIn)As/GaAs structures are receiving considerable attention because of their applications in high speed devices [1–3], and the interest in fundamental studies of the stability of such strained structures [4,5]. In processing such structures, ion implantation is an important step; however, it introduces damage and additional strains. Myers and coworkers [6] have carried out extensive characterization of keV ion-implanted strained-layer-superlattice (SLS) structures. MeV ions also have potential applications for processing devices with strained-layer structures. Such MeV ion implantation introduces far less damage in the device-important surface layers compared to low energy (keV range) ion implantation (although about the same total damage is introduced throughout the implanted region). Also, MeV energies drive the implanted dopants much deeper. The dominant defect species produced in the surface layers by MeV ion implantation consist of a high density of point defects and their clusters [7] as opposed to the more heavily disordered and amorphous regions which are produced by keV ion implantation. Therefore, it is interesting to investigate the effects of MeV ion bombardment on strained epitaxial layer structures. We have studied the responses of strained epitaxial layers to MeV ion implantation damage using the double crystal diffraction X-ray rocking curve (XRC) and Raman

(wavelength = 514.5 nm) techniques [10]. The results are presented in this paper.

2. Experimental technique

Ga_{1-x}In_xAs single layers were grown, by molecular beam epitaxy, on semi-insulating GaAs(001) substrates held at approximately 550 °C, on which a 0.5 μm thick GaAs buffer layer was first grown. The as-grown samples were characterized by the XRC (Cu K α_1 radiation) and Raman techniques before they were bombarded with various MeV ions. In table 1, we list the sample (by number and by an alphabetical symbol also used in the figures) and then the x -value (In composition fraction) and thickness h are given. The last column lists the various ions and energies used in the subsequent bombardment. The indium content in the epitaxial layer obtained by the XRC analysis, $x(\text{XRC})$, is listed in the fourth column and tends to be smaller than the nominal content x for most samples. There has been considerable discussion of the critical thickness of strained epitaxial films. The critical thickness h_c calculated under equilibrium conditions [8] is listed in table 1 and in parenthesis we list the values calculated with an energy balance model motivated by metastable SiGe layer results [9]. Note the large difference between the values, and that our samples have thicknesses of the same order of magnitude as those calculated with the energy bal-

Table 1

Characteristics of the as-grown $\text{Ga}_{1-x}\text{In}_x\text{As}$ layers are given. Listed below are the sample number, nominal composition (x), nominal thickness (h), composition estimated from the X-ray data ($x(\text{XRC})$), critical thickness (h_c), in-plane X-ray strain (ϵ_1^{Xr}), misfit (ϵ_f), perpendicular elastic strain (ϵ_{zz}), measured LO frequency (LO), bulk-equivalent LO frequency (ω_0), and the ion beam used.

Sample	x	h (nm)	x (XRC)	h_c (nm)	ϵ_1^{Xr} (%)	ϵ_f (%)	ϵ_{zz} (%)	LO (cm^{-1})	ω_0 (cm^{-1})	Ion beam
387 (g)	0.10	150	0.095	15 (298)	< 0.01	0.67	0.63	291.3	289.1	2 MeV He
389 (h)	0.10	250	0.093	16 (313)	0.32	0.66	0.32	290.0	288.9	2 MeV He
509 (a)	0.12	110	0.102	14 (251)	< 0.01	0.74	0.67	292.2	289.8	9 MeV P
520 (b)	0.12	140	0.089	17 (346)	0.02	0.64	0.56	291.9	289.9	9 MeV P
519 (c)	0.12	170	0.089	17 (343)	0.03, 0.05	0.64	0.55	291.3	289.4	9 MeV P
508 (d)	0.12	200	0.088	17 (357)	0.07, 0.09	0.64	0.50	291.6	289.8	9 MeV P
510 (e)	0.12	250	0.102	14 (256)	0.21, 0.26	0.73	0.44	290.6	289.0	9 MeV P
1	0.07	100	0.084	18 (396)	< 0.01	0.60	0.55	291.8	289.9	15 MeV Cl
2	0.07	1000	0.071	22 (597)	0.39	0.51	0.10	289.9	289.6	15 MeV Cl
3	0.15	1000	0.107	13 (224)	0.66	0.77	0.10	288.3	288.0	15 MeV Cl

ance model. Those samples with a measured in-plane mismatch, ϵ_1^{Xr} , of less than 0.01% are regarded as pseudomorphic in this paper, and these measured values are listed in the sixth column of table 1.

The MeV ion irradiations were performed at room temperature with doses ranging from 5×10^{12} to 5×10^{15} ions/ cm^2 . The particle beam currents were about 0.8–1 μA for the 2 MeV He beam, 10 nA for the 15 MeV Cl beam, and 2.5–10 μA for the 9 MeV P beam. The rather high beam current for the 9 MeV P beam caused a significant beam-heating effect. The estimated beam-induced temperature rise was about 300 °C [10]. The estimated projected range [11] in GaAs is about 6.3 μm for 2 MeV He, 4.0 μm for 9 MeV P, and 5.3 μm for 15 MeV Cl beam. It is assumed that the MeV ion damage and induced strain are uniform in depth for the epitaxial layers with thicknesses up to 1 μm [15].

3. Results and discussion

X-ray rocking curves measure the lattice spacings of the epitaxial film relative to the undamaged part of the substrate, in the direction normal to the surface and in the two in-plane directions. From the lattice spacings, the elastic strains can be calculated under the assumption that a biaxial stress exists in the film [16]. We write the elastic strain (in the [001] direction perpendicular to the planar face) in an ion-damaged strained epitaxial layer as

$$\epsilon_{zz}(x, D) = \epsilon_{zz}(x, 0) + \Delta\epsilon_{zz}(D), \quad (1)$$

where the first term on the right hand side is due to misfit in the as-grown undamaged layer and the second term is the beam-induced change. For the three pseudomorphic samples (i.e., samples with the in-plane mismatch of less than 0.01%), in fig. 1 we plot the strain in the damaged strained epitaxial layer as a function of

damage-energy deposition (which equals the beam dose times the nuclear stopping power). Since, at the ion energies used in the present study, the nuclear stopping power is approximately constant over a depth of about 1 μm from the surface, we assume a uniform nuclear stopping power within the epitaxial layer and use its value at the surface (which can be found from the stopping power table [11] at the incident ion energy) in

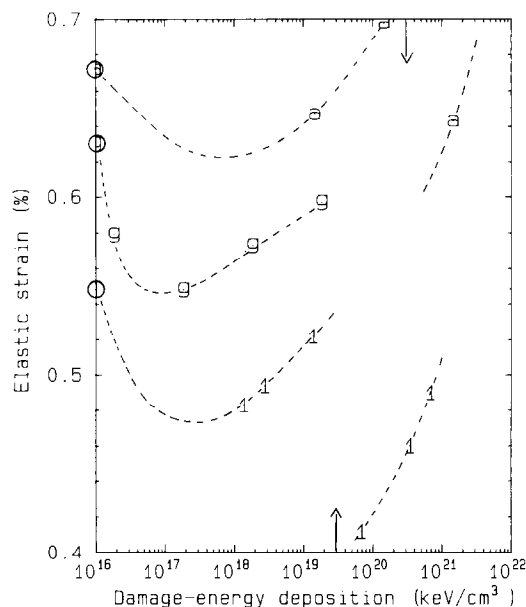


Fig. 1. The perpendicular elastic strain, ϵ_{zz} , of the damaged epitaxial layer is plotted for three pseudomorphic films as a function of the damage-energy deposition. The data symbols are listed in the first column of table 1. The two vertical arrows indicate the approximate positions of precipitous perpendicular strain release. The sample with data symbols “a” was bombarded with 9 MeV P, “g” with 2 MeV He, and “l” with 15 MeV Cl.

calculating the damage energy deposition. At low ion doses the elastic strain decreases with increasing beam dose, until a damage-energy deposition of 5×10^{16} – 5×10^{17} keV/cm³ is reached. Above this value of damage-energy deposition, the elastic strain increases with increasing dose, as fig. 1 shows. The 9 MeV P and 15 MeV Cl ion-bombarded samples show a precipitous strain release at a damage energy deposition of around 3×10^{19} and 3×10^{20} keV/cm³, respectively. The rough values of critical damage-energy deposition are indicated by vertical arrows in fig. 1. The maximum beam dose, 5×10^{15} ions/cm², for 2 MeV He ions (data symbol = "g") was not high enough to exceed this critical volume of damage energy deposition. The factor of 10 higher damage-energy deposition for P ions than for Cl ions to cause precipitous strain release is probably due to the beam heating by the P beam induced by the high beam currents.

A precipitous stress release phenomenon was observed by Myers and coworkers [6] in ion-implanted (GaIn)As/GaAs strained-layer superlattice (SLS) samples. Their electron microscopy studies revealed that the stress release was accompanied by the formation of a dense dislocation network at the (GaIn)As–GaAs interface. However, from our measurements, the in-plane mismatch for the initially pseudomorphic samples did not increase beyond the XRC detectability limit (0.01%) at all beam doses. Arnold and coworkers [18] used 320 keV Kr ions and 150 keV Si ions to implant GaInAs/GaAs and GaAsP/GaP strained layer superlattices (SLS) and reported a stress-relief (similar to strain-relief) phenomenon. Their damage-energy deposition of $\sim 2 \times 10^{20}$ keV/cm³ at the stress-relief is comparable to our 9 MeV P bombarded sample for which it is 2 – 4×10^{20} keV/cm³ (assuming that their beam current was relatively high and induced some beam heating as for our P ions). Since the types of implant-induced defects in the epitaxial layer or in the SLS samples are mainly extended defects and disordered regions for the keV ions in contrast with the point defects and their complexes for the MeV ions, this comparison suggests the damage-energy deposition at the point of stress (or strain) relief appears to depend only on the substrate temperature during implantation (including the beam heating effect), but not on the types of majority defects created in the epitaxial layer.

We also comment on the strain reduction observed in the low fluence region in fig. 1. If the implant-induced strain reduction (of about 0.08% for the 2 MeV He bombarded sample), at a damage-energy deposition of less than 5×10^{16} – 5×10^{17} keV/cm³, is not due to a beam-induced change in composition of the GaInAs layer, this may indicate that a simultaneous ion-bombardment during the strained epitaxial layer growth may be advantageous for thicker layer growth.

We now discuss our Raman scattering results. The

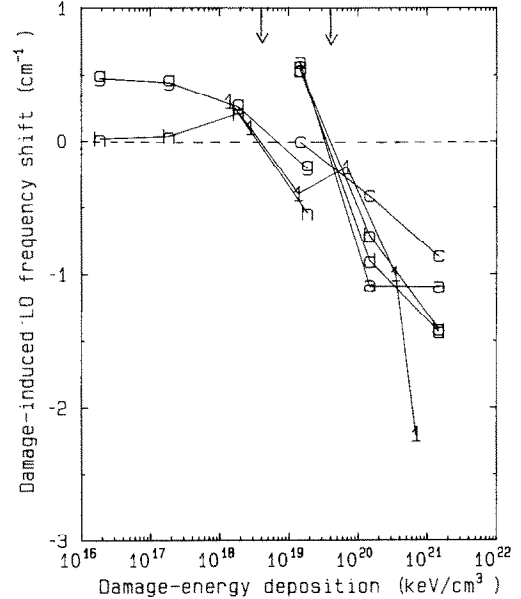


Fig. 2. The damage-induced LO phonon frequency shift, $\Delta\omega(D)$, obtained by subtracting the bulk-equivalent frequency of an undamaged film and the strain-induced shift from the total measured frequency [see eq. (2)] is plotted versus ion dose. The two vertical arrows indicate approximate positions of transition from positive to negative frequency shift.

total LO phonon frequency in an ion-damaged strained crystal is expressed approximately as

$$\Omega(x, \epsilon, D) = \omega_0(x) + \Delta\omega(\epsilon) + \Delta\omega(D), \quad (2)$$

where the first term on the right hand side is a bulk-equivalent frequency for undamaged crystal [12], the second term is the Raman shift induced by the strain due to the lattice mismatch and ion-damage (see eq. (1)), and the third term is the beam-induced shift minus the beam-induced strain contribution. The strain-induced Raman shift is calculated from the measured elastic strain in the ion-bombarded sample by [13,17]

$$\Delta\omega(\epsilon) = [p\epsilon_{zz} + q(\epsilon_{xx} + \epsilon_{yy})]/2\omega_0, \quad (3)$$

where p and q are the deformation constants and ϵ_{xx} , ϵ_{yy} and ϵ_{zz} are the elastic strains in [100], [010] and [001] directions, respectively. The LO frequency, $\omega_0(x)$, is obtained by subtracting the strain contribution from the Raman data in the as-grown samples [12]. This frequency is a function of the layer composition, and is listed in table 1.

From the frequency Ω measured from the damaged crystal, we subtract the composition-dependent frequency $\omega_0(x)$ and the strain contribution $\Delta\omega(\epsilon)$ to obtain the frequency induced by ion damage only. In fig. 2, we present the damage-induced shift $\Delta\omega(D)$, as a function of damage-energy deposition. The data symbols and the ion beams all correspond to the samples given in table

1. The dashed horizontal line represents the phonon frequency of the undamaged as-grown samples. The data points above zero at the lower doses, although they are only above zero by a small amount, systematically indicate an increase in the Raman frequency from the unbombarded sample values. At higher doses, the frequency decreases as expected for the ion-damaged GaAs crystals [14]. The damage-energy deposition, at the transition from positive to negative frequency shift, is roughly 4×10^{18} keV/cm³ for the 2 MeV He and 15 MeV Cl ion beams, and 4×10^{19} keV/cm³ for the 9 MeV P beam (positions are indicated by arrows in the figure). The order of magnitude higher damage energy deposition level for the 9 MeV P beam is probably due to the bombarding beam heating effect, consistent with the damage-energy deposition level at the precipitous strain release seen in fig. 1, and already discussed. The large energy flux of the P ion beam, which probably increased the target temperature significantly, seems to cause a delayed damage-effect both in the precipitous strain release (see fig. 1) and in the Raman frequency decrease (see fig. 2).

In order to compare with the responses of the strained unrelaxed samples, we bombarded some samples with

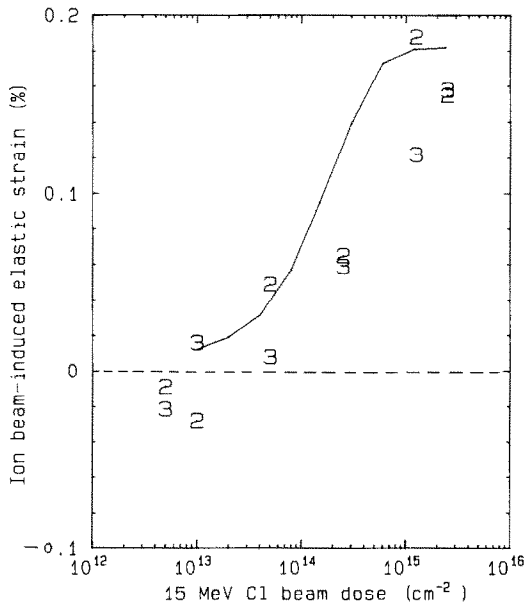


Fig. 3. The beam-induced perpendicular elastic strain, $\Delta\epsilon_{zz}(D)$, obtained from the total measured perpendicular elastic strain [17] by subtracting the perpendicular elastic strain in an unbombarded as-grown sample [see eq. (1)] is plotted versus ion dose. Data are given for the two $1 \mu\text{m}$ thick, well-relaxed samples, "2" and "3" in table 1. The solid curve is for a bulk GaAs(001) crystal bombarded with the same ion (taken from ref. [7]). This figure shows that the $1 \mu\text{m}$ thick, well-relaxed layers behave similarly to bulk GaAs(001) crystals under ion bombardment.

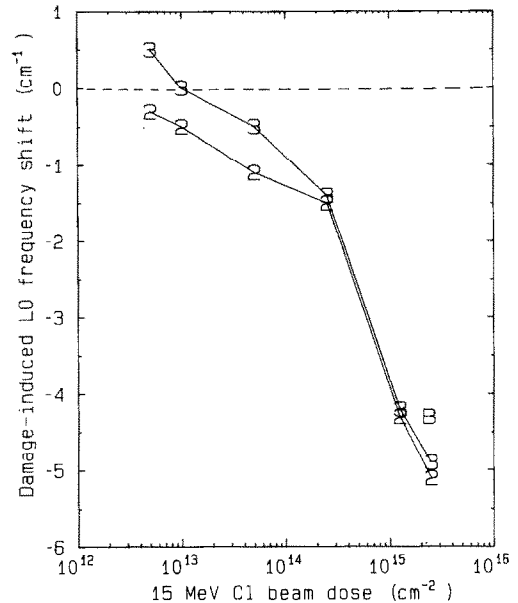


Fig. 4. For the $1 \mu\text{m}$ thick, well-relaxed (GaIn)As films, the damage-induced LO phonon shift, $\Delta\omega(D)$, is plotted as a function of ion dose. The data point "B" indicates the LO shift in a bulk GaAs(001) crystal under the same ion bombardment (taken from ref. [11]).

well-relaxed epitaxial layers. In figs. 3 and 4, the damage-induced elastic strain and Raman shifts are shown as a function of 15 MeV Cl ion dose for $1 \mu\text{m}$ thick $\text{Ga}_{1-x}\text{In}_x\text{As}$ layers with $x = 0.07$ and 0.15 (samples 2 and 3 in table 1). The initial lattice-relaxation in these films was such that the in-plane mismatch was $0.76\epsilon_f$ for $x = 0.07$ film and $0.86\epsilon_f$ for the $x = 0.15$ film. In these well-relaxed layers, the beam-induced elastic strain, $\Delta\epsilon_{zz}(D)$, which is shown in fig. 3 and the damage-induced phonon shifts, $\Delta\omega(D)$, which is shown in fig. 4, behave similarly to those observed in a bulk GaAs(001) crystal bombarded with 15 MeV Cl ions [7,14]. The bulk GaAs data are shown by a solid line in fig. 3 for the elastic strain and by the data symbol B in fig. 4 for the Raman shift. In both figures, the horizontal line represents data for as-grown layers before bombardment. At low ion doses, a small negative shift in the elastic strain and a positive shift in the Raman frequency are again observed.

4. Summary

We have presented data on the elastic strains and LO phonon shifts in MeV ion-damaged strained $\text{Ga}_{1-x}\text{In}_x\text{As}$ layers of various thickness on GaAs. A beam-induced decrease of elastic strain was observed at a lower fluence range, which may prove advantageous

in ion-implantation processing of strained layers and SLS samples or in the growth of strained systems by using simultaneous ion-bombardment. In layers with no observable in-plane mismatch (less than 0.01%), a precipitous strain release phenomenon is observed at a damage-energy deposition of about 3×10^{19} keV/cm³. A negative Raman frequency shift is observed at damage-energy depositions higher than about 4×10^{18} keV/cm³. For a very high beam current (the 9 MeV P beam), the corresponding damage-energy deposition levels (for similar effects) were higher by roughly an order of magnitude. Well-relaxed layers show beam-induced shifts in strain and in Raman frequency which are similar to those observed in ion-damaged bulk GaAs crystals.

The SUNY-Buffalo portion of the work was supported by the Office of Naval Research under the contract number N00014-87-K-0799. C.R. Wie thanks his graduate students H.M. Kim and K. Xie for carrying out the rocking curve measurements.

References

- [1] J.J. Rosenberg, M. Benlamri, P.D. Kirchner, J.M. Woodall, and G.D. Pettit, IEEE Electron Dev. Lett. EDL-6 (1985) 491.
- [2] H. Ito and T. Ishibashi, Jpn. J. Appl. Phys. 25 (1986) L421.
- [3] L.P. Ramberg, P.M. Enquist, Y.-K. Chen, F.E. Najjar, L.F. Eastman, E.A. Fitzgerald, and K.L. Kavanagh, J. Appl. Phys. 61 (1987) 1234.
- [4] B.W. Dodson and J.Y. Tsao, Appl. Phys. Lett. 51 (1987) 1325.
- [5] P.L. Gourley, I.J. Fritz and L.R. Dawson, Appl. Phys. Lett. 52 (1988) 377.
- [6] D.R. Myers, G.W. Arnold, C.R. Hills, L.R. Dawson, and B.L. Doyle, Appl. Phys. Lett. 51 (1987) 820, and references therein.
- [7] C.R. Wie, T.A. Tombrello and T. Vreeland, Jr., Phys. Rev. B33 (1986) 4083.
- [8] J.W. Matthews and A.E. Blakeslee, J. Cryst. Growth 27 (1974) 118.
- [9] R. People and J.C. Bean, Appl. Phys. Lett. 47 (1985) 322.
- [10] C.R. Wie, K. Xie, H.M. Kim, J.F. Chen, G. Burns, F.H. Dacol, G.D. Pettit, and J.M. Woodall, SPIE Proc. vol. 946 (1988).
- [11] L.C. Northcliffe and R.F. Schilling, Range and Stopping Power Table for Heavy Ions, Nuclear Data Table 7, No 3-4 (Academic Press, New York 1970).
- [12] G. Burns, C.R. Wie, F.H. Dacol, G.D. Pettit, and J.M. Woodall, Appl. Phys. Lett. 51 (1987) 1919.
- [13] F. Cerdeira, C.J. Buchenauer, F.H. Pollak, and M. Cardona, Phys. Rev. B 5 (1972) 580.
- [14] G. Burns, F.H. Dacol, C.R. Wie, E. Burstein, and M. Cardona, Solid State Commun. 62 (1987) 449.
- [15] See, for example, Figure 1 and Figure 4 of ref. [7].
- [16] Details for calculating the elastic strains from the x-ray rocking curve data are described in C.R. Wie, H.M. Kim, and K.M. Lau, SPIE Proc. vol. 877, p. 41 (1988).
- [17] Parallel elastic strains can be obtained from $\epsilon_{zz}/\epsilon_{xx} = 2\nu/(1-\nu)$ where ν is the Poisson ratio.
- [18] G.W. Arnold, S.T. Picraux, D.R. Myers, D.L. Doyle, P.S. Peercy, R.M. Biefeld, and L.R. Dawson, Mater. Res. Soc. Symp. Proc. vol. 77 (1987) 417.